Time-of-flight imaging for assessing soil deformations and improving forestry vehicle tracking accuracy

Lari Melander[a]* and Risto Ritala[a]

[a]*Automation and Hydraulic Engineering, Tampere University of Technology, Tampere, Finland;*

Lari Melander, +358503266652, lari.melander@tut.fi, Korkeakoulunkatu 10, 33720 Tampere.

Time-of-flight imaging for assessing soil deformations and improving forestry vehicle tracking accuracy

Automatically collected forest environment data is essential when developing more accurate and efficient forestry operations. Reliable position-based data enables efficient wood procurement operations and helps to avoid damage to the forest floor. A modern forestry vehicle with extensive sensing capabilities could measure environmental parameters, such as soil type, topography or weather conditions, while carrying out other wood procurement tasks. Furthermore, methods to improve positioning accuracy are also called for when the positioning is based on global satellite navigation systems (GNSS), whose signals are often blocked by the forest canopy. In this paper, data is collected automatically with two of Microsoft's Kinect v2 time-of-flight sensors during field tests in a forest environment in Southern Finland. The aim of the paper is to propose methods which will improve positioning accuracy by enabling the movements of the forwarder to be detected and also to provide reliable measurements of any soil deformations caused by the vehicle in real time. The results show that Kinect v2 technology enables tracking of the vehicle's movements over short distances with sub-meter accuracy, thus supporting the GNSS positioning during the short periods of unavailable satellite visibility. Kinect v2 technology has also been shown to be able to measure the depth of ruts as accurately as conventional manual measurements.

Keywords: Kinect v2; time-of-flight; depth camera; heavy forestry vehicle positioning

Introduction

Detailed forest resource management, or precision forestry, means that various modern technologies are used to gather information about the forest so that its characteristics can be determined accurately with high spatial resolution (Holopainen et al. 2014). Such information maximizes the efficiency of forestry operations and minimizes any permanent impact on the forest floor. Much recent research has been based on the vast amounts of positioning data gathered from the field operations of modern cut-to-length harvesters (Oliviera et al. 2016). One particular field of interest is how to combine the harvester data with data from remote sensing, such as airborne laser scanning (ALS), to record accurate single-tree data (Lindroos et al. 2011; Holopainen et al. 2014).

A forestry vehicle is a potential platform for automatically collecting data about the forest environment while carrying out normal wood procurement tasks. Among the parameters of particular interest are the soil's characteristics, such as its type, moisture content and topography. A modern forest vehicle could also collect other data on spatially or temporally varying parameters, such as the weather conditions. Automatically collected data about the above characteristics would enable the development of new applications for improving the quality of forest operations. For example, traversability estimates based on detailed information about the forest's resources and operating conditions could be used for routing the forwarder. Data about soil deformations, for instance, which used to be collected manually, could be collected and processed automatically for real time usage and better coverage over the driven routes.

In order for the data about the environmental parameters to be used efficiently in Geographical Information Systems (GIS) it must be positioned accurately. Most heavy forestry vehicles are positioned with one or other of the three available global navigation satellite systems

(GNSS): the United States' Navstar Global Positioning System (GPS), Russia's GLONASS and Europe's Galileo system. The system used, and the receiver technologies, can have a significant effect on positioning accuracy, as can the forest conditions, which obviously affect how well the vehicle receives the satellite signals. It is well known that satellite positioning of a moving vehicle under a forest canopy is difficult because the signal is sometimes blocked and thus temporarily unavailable, resulting in sudden position jumps or multipath signals. Many studies have evaluated the positioning systems and the effect that the forest canopies have on their positioning accuracy (Holden et al. 2001; Lindroos et al. 2011; Dawidowicz & Krzan 2014; Bakuła et al. 2015; Kaartinen et al. 2015; Blum et al. 2016). It has been shown that systems using devices which combine two or more satellite systems, e.g. GPS and GLONASS, perform better than single-technology devices when there is virtually no direct view of the sky (Dawidowicz & Krzan 2014; Blum et al. 2016). Many studies have focused on achieving the sub-meter accuracy required for single-tree positioning (Lindroos et al. 2011; Ringdahl et al. 2011). If the exact position of the harvester head were known, the single-tree information gathered by a modern cut-to-length harvester could be linked to the tree's location. With an integrated Real-Time Kinematic (RTK) GNSS system on a harvester, it would indeed be possible to position single trees with sub-meter accuracy (Hauglin et al. 2017). It is generally accepted that for open land surveys, RTK-GNSS systems are the most accurate GNSS technologies available. However, so far no studies on RTK-GNSS devices operating under forest canopies have achieved sub-meter accuracy (Bakuła et al. 2015; Kaartinen et al. 2015). Nevertheless, there have been some significant developments. Some researchers have shown that it is possible to increase the positioning accuracy under a forest canopy by equipping the vehicle with additional sensors, such as inertial measurement units (IMUs) (Kaartinen et al. 2015) or LiDAR (Qian et al. 2017).

Ringdahl et al. (2011) used a gyroscope to compensate for the movement of the GNSS device when the vehicle is at an angle on the often uneven forest terrain. This also improves the accuracy of the vehicle positioning.

So, previous studies have shown that positioning accuracy can be improved to the level required, but it requires either clear satellite signal paths or the installation of additional sensors to the vehicles. Therefore, attention is now focusing on low-cost sensor solutions for improving positioning accuracy. These are needed in, for example, thinning operations, during which the forest canopies most interfere with the GNSS positioning system. The precise position of the vehicle's body is needed to obtain reliable soil measurements, whereas it is the position of the harvester head that is needed for single-tree positioning.

There are a number of different sensors on the market for measuring the forest environment automatically during forest operations. Of particular interest is the use of laser scanners, which can be used to identify and measure the characteristics of individual trees and for measuring the terrain (Schmid et al. 2004). However, laser scanner systems are rather expensive components for forestry vehicles. Photogrammetric systems have been proposed for measuring wheel ruts (Haas et al. 2016; Pierzchata et al. 2016), but no such automated solutions have yet been integrated into forestry vehicles. These systems are less expensive than laser scanners, but their applications are restricted. They are affected by the ambient light, by their inability to see below the surface of any water in the wheel ruts and by the difficulty of mounting the cameras on the vehicle. There is another 3D measurement technology, however, which has not been much studied in forestry applications. This technology is time-of-flight depth imaging, which determines distances by illuminating the scene with modulated light and observing the time taken for the light to reflect back from the target (Foix et al. 2011). The travel time is translated into a distance measure for each pixel in the camera sensor. Although time-of-flight technology shares some of the drawbacks of photogrammetry, like the inability to penetrate water surfaces, it is far less prone to changes in the ambient light because it utilises near-infrared ranges.

The first version of Microsoft's Kinect imaging device has been widely tested in many fields, including forestry and agricultural applications (Marinello et al. 2015), but the sensor did not use time-of-flight technology and was reported to be unusable in direct sunlight (Zennaro et al. 2015). The second version, Kinect (v2), uses an infrared camera and illumination for the time-of-flight measurements and is one of the most efficient low-cost depth camera sensors available, see e.g. (Butkiewicz 2014; Fankhauser et al. 2015; Zennaro et al. 2015; Pagliari et al. 2016; Rosell-Polo et al. 2017). The Kinect v2 sells for 100-200€, which is significantly lower than the price of any other time-of-flight or LiDAR measurement systems on the market. The Kinect v2 camera provides three outputs from its sensors. The color camera sensor records RGB color images with a resolution of 1920×1080 pixels, and the infrared sensor produces greyscale images and depth images with a resolution of 512×424 pixels. The fields of view are 84.1×53.8 degrees and 70×60 degrees, respectively (Microsoft 2017). The Kinect v2 has been tested outdoors in coastal mapping (Butkiewicz 2014), mobile robot navigation (Fankhauser et al. 2015), and terrestrial laser scanning (Rosell-Polo et al. 2017), and has proved to be much more robust than the first version. Pagliari et al. (2016) have reported on outdoor navigations that combine the Kinect v2 with GNSS measurements. Corti et al. (2016) found that the optimal Kinect v2 measuring range is between one and three meters, with an approximate measurement accuracy of 10mm. Furthermore, they found that the color of the target material has little effect on the accuracy of the measurements, although temperature variations may cause some errors. Yang et al. (2015) obtained a cone model for the depth accuracy of the Kinect v2 which showed that, within the ranges covered in their study, it had a margin of error of less than 4 mm for indoor depth measurements. Before the on-machine field tests reported in this paper, the most suitable measuring range for Kinect sensors has been determined in preliminary forest ground measurements. Indeed, our preliminary tests confirmed that the Kinect v2 has the potential to measure outdoor terrain at distances of between one and two meters. Our preliminary measurements are not reported here as they are completely in line with the results from earlier studies (Butkiewicz 2014; Fankhauser et al. 2015; Hernandez-Aceituno et al. 2016).

This paper presents a study of the use of the Kinect v2 time-of-flight 3D imaging device, (designed for indoor use), as an automated outdoor measurement device for forestry operations. Earlier studies do indicate that Kinect's optimal measuring range and accuracy, and its sensitivity to changes in temperature and ambient light are sufficient for our intended application. Therefore, our overarching aim was to test whether the device can produce suitably accurate measurements of the relevant forest parameters when mounted on a forwarder in a real forest environment. The detailed aims were: i) to measure the topography of the immediate environment around the forwarder, in particular the wheel tracks; and, ii) estimate the velocity and position of the forwarder independently of the GNSS measurements, in order to improve the positioning accuracy under forest canopies.

Materials and methods

We mounted two Kinect cameras on a forwarder operating in a real forest environment in Southern Finland in order to carry out our field tests. We were able to confirm Kinect's ability to measure forest soil topography by comparing its measurements for rut depth with manual ones. In addition, its velocity and position measurements were compared to those from the forwarder information system and the on-board GNSS device.

Kinect measurement system

The measurement system for this continuous data collection consisted of two shielded Microsoft Kinect for Windows v2 sensor units attached to the rearmost bunk of the forwarder trailer (Figure 1a). There was a shielded measurement computer inside the forwarder's body for data collection (Figure 1b). The Kinect sensors were protected with a purpose-built steel box with one side open to allow for recording the images. This open side was protected with a 6mm thick Lexan Margard MR5E polycarbonate sheet (SABIC 2017), identical to the protective covers used in the cabin windows of forestry vehicles. This window was firmly attached against the Kinect's measuring face, firstly to prevent the accumulation of moisture and secondly to avoid infrared flash reflections from the interface between the camera lens and the protective window. Kinect USB and power cords were fed to the measurement computer through a plastic cable duct (Figure 1b).

<Placeholder for Figure 1>

Figure 1. Kinect measurement system in the forwarder.

The computer was an Intel NUC minicomputer running the Ubuntu 16.04 LTS operating system. A Robotic Operating System (ROS) framework (Quigley et al. 2009) was used to connect the computer with the Kinect device. The Kinects were calibrated before the field tests and the image feeds were recorded with the open-source package iai_kinect2 (Wiedemeyer 2015).

In the configuration described here, the wheel is partially blocking the Kinect's field of view, but this is due to a practical constraint, i.e. the bunk above the rearmost wheels of the trailer can support the down-facing cameras without the need for any additional supporting structures. Both of the Kinects were mounted approximately 1.7 meters above the ground. The sensors were aligned to face down perpendicularly to the ground, thus minimizing the measuring distance in order to optimize the device's outdoor performance. The sensors were 2 meters apart horizontally (Figure 1b), which is almost the same as the gap between the forwarder's tracks. In our configuration, there is no overlap in the fields of view of the two Kinects, so there is a narrow strip of ground area between the wheels which is not recorded (Figure 1b). One final consideration is that the GNSS receiver is located on the roof of the forwarder cabin (Figure 1a), which means that there is an offset of up to 7.8 meters between the receiver and the Kinect sensors when the front part of the forwarder is in line with the trailer.

The field tests recorded all three types of Kinect images, i.e. RGB, infrared and depth. The maximum sampling frequency of the Kinect v2 is 30 Hz, but in order to save disk space on the measurement computer a sampling frequency of 10 Hz was used. This was considered to be sufficient for aligning consecutive images given the speed of the forwarder. The average speed of the forwarder in the field tests was around 3 km/h. The RGB image was recorded at a reduced resolution, i.e. 960×540 pixels, which is one quarter of the full available image size; again to save disk space. The infrared and depth images were recorded at their full resolution. The amount of data stored on the disk increased by 1.5 Gb a minute with these image sizes and sampling frequency.

Test area, equipment and other measurement outputs

The test tracks were located in Vihti, in Southern Finland. The test area was an approximately 100-meter long forest logging road which had been opened up by a harvester 6 months earlier for other trials. Three 20-meter long straight test tracks were constructed along this logging road. The starting points of the test tracks were marked, and the 20-meter distances were measured by hand. A mark was painted on the ground at one-meter intervals along the tracks. The rut depths after the forwarder had passed were measured manually with a measurement rod. The rod was a 160 cm-wide tool that was placed perpendicularly over the track. Then the depth of the rut was measured from the center of the rod using a ruler. The rut depth was measured in relation to the level of the surrounding ground 80 cm around from the center of the rut. The logging road was driven over once in both directions, giving a total of six 20-meter test track runs. The forwarder was an unladen Ponsse Elk 8W equipped with wheel chains. Most of the soil deformation had been caused by the tests which had been conducted earlier on the same track, when the tracks had been driven over several times by a harvester and a forwarder with medium-sized loads.

The field tests were conducted on a typical November day in Southern Finland. The temperature was close to zero, the sky was dark and overcast and there was a little rain and sleet. However, the ground was free from snow and frost. The soil was quite sandy, which is typical of this area of forest. The first track was fine, sandy moraine, and the second track was medium-fine sandy moraine. However, the third track consisted of loamy fine and medium-fine sand, so while the first track was dry and had not suffered from subsidence, the third one was mainly wet and had suffered large deformations. The second track had been treated earlier with coniferous litter, so its condition was somewhere between that of the first and third tracks.

In addition to the Kinect measurements, the forwarder's CAN bus data with GNSS measurements were collected using the Ponsse Opti7 integrated on-board computer system. CAN bus is a communication standard for linking different devices together. It is used widely in off-road vehicles for transferring sensor measurements and controlling actuators. The forwarder speed, calculated from the power transmission, was used from the CAN bus data set. The sampling time of the CAN bus was 20 ms. The forwarder stopped before each test track, allowing time for the synchronization of the Kinect images and the CAN bus measurements.

Image-based analysis for speed and heading

The Kinect images were analysed off-line using Matlab R2015b software, and from this analysis we were able to develop some algorithms which are suitable for forestry applications. Throughout this study, the Kinect depth data is used to construct metric measurements based on the acquired distances (depth image pixel values) and the field-of-view angle of the Kinect v2. The metric field of view for the image can be calculated using basic trigonometry as in equation 1,

$$FOV_m = 2 * D * tan(\frac{FOV_{angle}}{2}) \quad (1)$$

where FOV_m is a metric field-of-view of the image in a vertical or horizontal direction with the camera distance D from the imaged target and the vertical or horizontal field-of-view angle, FOV_{angle}. The size of the infrared images in metres can be easily calculated with this approach, as the infrared and depth images are produced by the same sensor.

To estimate speed, the offset between the consecutive infrared images is divided by the time difference of the image time stamps. In this paper, the offset is evaluated with the 2D normalized cross-correlation function in Matlab (Lewis 1995). This function slides the compared images over each other pixel by pixel, calculates the cross-correlation coefficient for each step and normalizes the results between 0 and 1; a coefficient of 1 meaning that identical images are compared. Rather than computing the cross-correlation over entire images, a small region, referred to as the measurement region, was cross-correlated. This reduces the effect of high noise at the image borders. To speed up the calculation, only 10% of the measurement region is used from the sequential image for the cross-correlation of the preceding image. A strong peak in the cross-correlation suggests that the compared image areas represent the same area on the forest floor. In our coordinate system, the Y-axis of the image is the direction in which the forwarder is heading, so only the speed along this axis is used. Therefore, the rotation is not taken into account when calculating the displacement of the image in a single camera. The angle shifts between the consecutive images are small due to the high sampling frequency relative to the speeds of the heavy forest vehicles.

Using two sensors allowed us to take an average of the parallel measurements for the final speed estimate. On the other hand, a difference in the speed measurements indicates that the forwarder is turning. Similarly, the difference in the distances travelled by the two rear wheels indicate a change in direction as in:

$$sin(\Delta\alpha_k) = \frac{D_{left,k} - D_{right,k}}{d} \quad (2)$$

where $\Delta\alpha_k$ is the angle change of the vehicle at time k from the parallel axis of the heading direction; $D_{left,k}$ and $D_{right,k}$ are the measured displacements of the left and right cameras; and d is the distance between the cameras. Positive angles indicate the forwarder trailer is making a right turn, and negative angles, a left one. A horizontal position change can be estimated by combining the estimates for speed and the change in heading.

The cross-correlation coefficient peak tends to vary between 0.85 and 0.98, depending on the image noise, camera vibration and the movement in the X-direction. Figure 2a presents a typical result: a clearly distinguishable peak at 0.95. The abscissa in Figure 2 is the offset in pixels as the cross-correlation template, created from the sequential image, slides over the measurement region in the preceding image.

<Placeholder for Figure 2>

Figure 2. Examples of the normalized cross-correlation results between two consecutive infrared images in Y-direction: (a) typical result and (b) degenerated result.

When the environment changes rapidly between the consecutive images, the cross-correlation results are poor. Figure 2b shows an example of such a degenerated cross-correlation function where all the coefficients fall far below 0.5, lacking a single clear peak.

A weak cross-correlation can cause a sudden change in the calculated image offset. Such a leap was taken to be an indicator of an unreliable motion measurement, in particular for the perpendicular direction of the forwarder motion. The motion estimate was considered unreliable if the change exceeded 10 pixels in the X direction or 100 pixels in the Y-direction. When one or other of these thresholds was exceeded, the speed estimate was held at its previous accepted value. Figure 3 shows the X and Y offsets from the third test track, where the puddles on the track occasionally rendered the cross-correlation method inaccurate.

<Placeholder for Figure 3>

Figure 3. Detected offsets between the consecutive images in the third-track test data.

In addition to the rapid environment changes, the varying topography of the forest ground will sometimes make the Kinects lean at an angle, thus differing the measurement geometry from the assumed perpendicular plane. Sideways inclinations are observed in the X-direction cross-correlation results, so they are considered as unreliable measurements, as explained above. The inclinations in the travel direction are visible in the Y-direction cross-correlation results as rapid peaks, which are removed with a median filtering.

To improve the reliability of the measurements in such difficult conditions, the cross-correlation was computed over three measurement regions of the infrared image. This approach provides three speed measurements for each image pair. In this study, the speed that was closest to the speed of the preceding measurement is chosen. This is justified by the high inertia of the heavy forestry vehicle. Figure 4 demonstrates the two different arrangements used in this study for the measurement regions.

<Placeholder for Figure 4>

Figure 4. Measurement regions for computing the cross-correlation.

The wider uniform white rectangle shows the single measurement region and the three grey rectangles show the three measurement regions.

3D mapping of the forest floor

Kinect depth images enable the generation of 3D point clouds from the measured profile of the soil surface. Figure 5 presents an example of the point cloud for one depth image with the X- and Y-axes being the image plane, and the Z-axis the distance between the sensor and the soil. The entire depth image is not used due to the noise at the image edges and the forwarder wheel being visible in the lower part of the image.

<Placeholder for Figure 5>

Figure 5. Soil surface profile as a 3D point cloud. The high-noise edge areas, and area with forwarder wheel have been removed.

However, the sampling rate ensures that the displacement in the direction of the forwarder movement is less than the area of the point cloud, so all the soil surface profile data is covered. An Iterative Closest Point (ICP) algorithm (Besl and McKay 1992) is commonly used for generating stitched 3D point cloud models from several consecutive point clouds. In this study, the ICP algorithm in Matlab (Matlab 2017) is used for evaluating the point cloud generation of the continuous wheel rut model.

A method for measuring the resulting rut depth directly on fixed measurement areas in the image was investigated, as an alternative to the full 3D modeling of the soil surface profile. The measurements can be computed in real time with the on-board computer, which makes the application more feasible for a forestry domain. It is reasonable to assume that the resulting rut depth is measurable at the center of each depth image. However, the distance of the camera from the ground varies when driving over the uneven forest floor. In our study, the ground base level is measured on the both sides of the depth image. Due to the small-scale topographic changes of the forest floor and other possible disturbances, such as tree branches, a small number of pixels is not sufficient to describe the actual rut depth or the ground base level. Therefore, a median from a larger area of depth pixels was taken. The sections chosen from the depth image are shown in Figure 6.

<Placeholder for Figure 6>

Figure 6. Depth image sections for the surface base level and rut depth measurements.

The selected sections are in the middle of the image, again to reduce the effects of the noisy borders in outdoor measurements. Due to the slight offset of the Kinect sensor to the forwarder rear wheel, the areas are not exactly the middle pixels of the full depth image.

Results

The RGB color images suffered from significant motion blur during the forwarder run, so they were less useful than the infrared images for the cross-correlation analysis, and were therefore discarded. The following results are based on only grayscale infrared images and the depth images.

Measured travel distances and speed of the forwarder

Table 1 shows comparison of the manual and the Kinect distance measurements every four meters on the different test tracks. The root-mean-square errors (RMSE) between the manual and Kinect measurements are also calculated to emphasize the difference between the test tracks. The distances reported are averages of the two Kinect sensor measurements, i.e. assuming straight motion. The distances are clearly more accurate with the three measurement regions, thus three cross-correlation results are combined, instead of just using one measurement region.

Table 1. Distances measured with one and three measurement regions in infrared images.

<Placeholder for Table 1>

Figure 7 shows the speeds recorded for the first two test tracks, where the results are similar using either one or three measurement regions in the infrared images. Figure 8 shows the differences in speed estimates for the third test track, where only the use of three measurement regions in the Kinect images provide results similar to the transmission system measurements throughout the data.

<Placeholder for Figure 7>

Figure 7. Measured speeds on test tracks one and two.

<Placeholder for Figure 8>

Figure 8. Measured speeds on test track three, using one and three measurement regions for the Kinect images.

The differences between the speed measurements are collected in Table 2. The mean of the true difference between the measurements is calculated to demonstrate the tendency of the Kinect and

GNSS measurements to be lower than the forwarder transmission measurements. The standard deviation is calculated to show that the difference varies depending on the track and the measurements. The numbers are consistent with the findings in the distance measurements and the use of three measurement regions returns more stable results in all of the tracks and running directions.

Table 2. Comparison between speed measurements.

<Placeholder for Table 2>

Position estimation of the forwarder

Figure 9 shows the estimated tracks separately for the GNSS and the Kinect measurements to emphasize their different nature if calculated independently of each other. Excluding the initial location and heading angle, the illustrated Kinect paths are generated based on Kinect data only. This means that the Kinect path will eventually drift further away from the true path as the measurement errors accumulate.

<Placeholder for Figure 9>

Figure 9. Forwarder position estimates using GNSS and Kinect measurements.

The calculated absolute difference for the final positions in the first and second runs were 10.45 and 10.82 meters respectively. Here, the GNSS final position was corrected to correspond to the position of the trailer, as shown in Figure 10. Although the Kinect positioning is capable of following the path through a 180 degrees turn, the final position difference clearly shows the drift of the Kinect positions. The RMS error between the GNSS and Kinect positions was calculated to show that the paths have similar differences in both running directions. The RMSE for the first and second runs were 7.30 and 5.84 meters respectively. As the GNSS position measurement itself was uncertain, the calculated RMSE should not be interpreted as the error between Kinect measurements and the ground truth.

Measured wheel rut depths after the vehicle pass

For the rut depth analysis it was not feasible to use the ICP algorithm to stitch the measured forest floor point clouds due to the long processing time and the increase in the memory requirements. With a regular desktop computer, the stitching of just two point clouds took several seconds while 50 point clouds took several minutes. The stitching process also accumulates errors, so the construction of the whole 20-meter path is not suitable for estimating the rut depths.

The results of the simpler depth measurements using fixed measurement areas of the images are shown in Figure 10, (left Kinect camera). The results are similar for the right camera. Figure 10 also reveals the different profiles of the test tracks. The Kinect measurements agreed with the manual measurements particularly well on test track three.

<Placeholder for Figure 10>

Figure 10. Measured wheel rut depths for the left side of the test tracks.

Table 3 presents the mean difference, standard deviation, and root-mean-square error of the depth measurements for each test track run. Manual measurements were taken at regular intervals of one meter, and the Kinect depth measurements were positioned with the Kinect distance estimate. The results indicate that the Kinect measurements are generally around 5 centimetres higher than the manual measurements and the variation in the measurements depends on the environmental conditions.

Table 3. Difference between the Kinect depth measurements and the manual measurements.

<Placeholder for Table 3>

Discussion

The Finnish Forest is a challenging environment for any image-based analysis, as the conditions affecting the measurements are far from controlled. It is challenging to take into account or compensate for the varying light, and other seasonal effects. There are many objects blown about by the wind and there are plenty of other disturbances, too. One of the main problems that we encountered was the unstable state of the soil structures, which can collapse under a sinking forwarder wheel. Freely flowing water displaced by the vehicle wheels was also a problem, as were other rapidly moving objects like swinging tree branches.

In spite of these challenges, the results show that at short distances of less than 20 m and with three measurement regions to reduce the interference of free water surfaces in the imaged area, Kinect is able to measure the motion of the forwarder reliably in logging road conditions. The accumulated distance calculated from the image displacements corresponds to the manual measurements with an accuracy of tens of centimetres over a distance of 20 m. As the errors of the distances are cumulative with our approach, the Kinect measurements should be used together with GNSS measurements for routing over longer distances. Our method for dealing with partially corrupted image data was found to be efficient. Using three measurement regions in the image (rather than one) improved the accuracy on all the test tracks, but it was particularly effective in removing all the false measurements caused by the difficult conditions on Track 3. Although image cross-correlation is not the ideal solution when there is rotation between the recorded images, the current results indicate that for slow-moving forestry vehicles, the cross-correlation is accurate enough for most practical purposes and the data can be computed in real time with practical sampling rates. We also found that filtering out the sudden peaks in the speed measurements when they exceed a given threshold is an efficient procedure for this application.

As is evident from Figure 3, large shifts in the X-direction tend to co-occur with unrealistic shifts in the Y-direction, so filtering the Y-direction shift with the X-direction shift appears to be justified.

When comparing the Kinect speed measurements to the GNSS and CAN bus measurements it is obvious that each of them has their own error sources. The GNSS measurements have errors resulting from blocked and multipath signals due to the forest canopies around the test tracks, but these errors are not accumulated over time. The recorded GNSS signal tends to jump between two points generating an erratic path and speed estimate. The speed estimate from the transmission system via the CAN bus is the best reference measurement for the Kinect speed measurements. The estimate is produced as an average of the wheel rotation speeds, and thus subject to integrated errors caused by slippage. As the results in Table 2 and Figure 8 show, the Kinect speed measurements tend to be lower than the CAN bus transmission measurements, in particular on the third test track. This is as expected, since the slipping in the soft soil causes the forwarder's wheels to spin faster, thus resulting in higher speed measurements. The difference between the Kinect and CAN bus speeds is thus an indicator for the driver of slippage and/or the risk of the vehicle sinking. This difference can be computed in real time at our sampling frequency, so it is a useful warning for the driver. The results also show that the GNSS speed measurement is lower than the transmission measurement, but the variation between these measurements is much higher than it is for the Kinect measurements. Overall, Kinect measurements using three measurement regions seem to offer the best performance for measuring both the distance and the speed of the forwarder.

The Kinect-based position estimate is also credible when the forwarder is turning. As long as the initial angle and position were set accurately, the forwarder path constructed from the velocity measurements followed the GNSS position measurements fairly closely. As the track in our tests was around 100 meters long including a total turn of 180 degrees, the difference of 10 meters in the final position is a reasonably good result. In practice, the positioning system would fuse the Kinect velocity measurements and the GNSS measurements into one position estimate, e.g. with a Kalman filter. The key to data fusion is to identify the situations where the GNSS measurements are compromised by the forest canopies, and in these cases the Kinect measurements should have a higher weight in the estimation. Further results need accurate GNSS measurements for the ground truth comparisons, but the results presented here suggest that Kinect is able to support positioning in thinning operations where the satellite signals could be blocked over long periods of time.

The Kinect infrared camera has enough resolution to take detailed measurements of variations in the surface profile in close range applications, and even enables the construction of a full 3D point cloud representing the forest soil surface after the forwarder has passed. The consecutive 3D clouds from the test tracks were registered and stitched together with the ICP algorithm. This algorithm is computationally heavy and thus slow, so it would have to be a post-processing operation in the current application. The errors are accumulated, since the consecutive images are stitched one after another, leading to obviously wrong results in the full 20-meter long test tracks. Point clouds were not directly applied for the wheel-rut depth estimation, but the track depth and ground base level were estimated at fixed measurement areas. The resulting wheel rut depth estimates were compared to the manual measurements performed for each meter of the test tracks. The results clearly show that the Kinect measurements return similar rut depth values to the manual measurements, although there seem to be some systematic errors throughout the compared data. The comparison in Table 3 showed that Kinect tends to overestimate the depth of the ruts compared to the manual measurements. The sensor height could affect the measurements, since it was found that the ground base level around the resulting rut is barely visible on the depth images. Therefore, it is possible that in cases where the vehicle is sinking heavily, the base level is measured from too narrow an area compared to the manual measurements.

There are other possible reasons for the systematic differences in the depth measurements. Firstly, the methods are slightly different. Kinect measures on top of the visible soil cover, which includes grass and other light organic materials. The rod and the ruler used in the manual measurements go deeper into the lightweight soil cover and water. This is especially noticeable in the depth measurements from the second test track, which had once been covered with coniferous litter. The third test track did not have much lightweight soil cover left, so for this track the systematic error is generally smaller, but other disturbances on the track produced a higher variance of the measurements. Secondly, both the measurement methods themselves can cause systematic errors. Kinect measures the soil surface through the shielded window, which can cause a permanent offset for the measurements due to the changed light travel time. The effect of this was minimized by making the polycarbonate window as thin and transparent as possible. The manual measurement process may also have shifted measurement values due to the methods of the measurer, e.g. where to place the ruler on uneven ground.

Our long-term objective is that all the computation and analyses should be done in the on-board computer of the forestry vehicle. The positioning estimates and the environmental measurements produced in this way would be of great value in forestry operations. Our image analysis methods can be computed within the image sampling time and are thus real-time functionalities.

The shielding structure constructed for the field tests worked well. However, the ventilation inside it is poor, whereas when the Kinect is used in indoor applications the device is freely ventilated with a stream of air. Although the restricted ventilation did not cause problems in our field tests, which were conducted outside in low temperatures, overheating may turn out to be more of an issue in summer conditions, and this would need further study.

Kinect also has the capability to record high quality color images. Although these are not suitable for estimating the motion of the vehicle, they could be useful in future applications for estimating soil properties based on color and texture for instance, or simply for documenting the forestry operation.

In conclusion, the Kinect has proved itself to be a versatile sensor capable of making automated forest environment measurements. The dedicated image-analysis algorithms and the use of the two protected Kinects were able to cope with the challenges of the forest environment, enabling the reliable estimation of the motion of the forestry vehicle and the depths of the wheel ruts. These results are from short-term field tests, so further studies are still needed to cover the device’s performance in long- term use in different types of forest conditions. Nevertheless, considering that the last test track (Track 3) was in such harsh condition that it would normally have been avoided by a forestry vehicle driver, the results indicate that the Kinect system appears to be usable, at least in the Finnish forest environment.

References

Bakuła M, Przestrzelski P, Kazmierczak R. 2015. Reliable Technology of Centimeter GPS / GLONASS Surveying in Forest Environments. IEEE Trans. Geosci. Remote Sens. 53:1029–1038.

Besl PJ, McKay ND. 1992. Method for registration of 3-D shapes. In: Proc. SPIE 1611, Sensor Fusion IV: Control Paradigms and Data Structures. Boston, MA. p. 586–606.

Blum R, Bischof R, Sauter UH, Foeller J. 2016. Tests of reception of the combination of GPS and GLONASS signals under and above forest canopy in the Black Forest, Germany, using choke ring antennas. Int. J. For. Eng. 27:2–14.

Butkiewicz T. 2014. Low-cost Coastal Mapping using Kinect v2 Time-of-Flight Cameras. In: Oceans - St. John's. IEEE. p. 1–9.

Corti A, Giancola S, Mainetti G, Sala R. 2016. A metrological characterization of the Kinect V2 time-of-flight camera. Rob. Auton. Syst. 75:584–594.

Dawidowicz K, Krzan G. 2014. Accuracy of single receiver static GNSS measurements under conditions of limited satellite availability Accuracy of single receiver static GNSS measurements under conditions of limited satellite availability. Surv. Rev. 46:278–287.

Fankhauser P, Bloesch M, Rodriguez D, Kaestner R, Hutter M, Siegwart R. 2015. Kinect v2 for Mobile Robot Navigation : Evaluation and Modeling. In: Advanced Robotics (ICAR), 2015 International Conference on. IEEE. p. 388–394.

Foix S, Alenya G, Torras C. 2011. Lock-in Time-of-Flight (ToF) Cameras: A Survey. IEEE Sensors J. 11:1917-1926.

Haas J, Ellhöft KH, Schack-Kirchner H, Lang F. 2016. Using photogrammetry to assess rutting caused by a forwarder—A comparison of different tires and bogie tracks. Soil Tillage Res. 163:14–20.

Hauglin M, Hansen EH, Næsset E, Busterud BE, Gjevestad GJO, Gobakken T. 2017. Accurate single-tree positions from a harvester : A test of two global satellite-based positioning systems. Accepted for publication in Scand. J. For. Res, http://dx.doi.org/10.1080/02827581.2017.1296967.

Hernandez-Aceituno J, Arnay R, Toledo J, Acosta L. 2016. Using Kinect on an Autonomous Vehicle for Outdoors Obstacle Detection. IEEE Sens. J. 16:3603–3610.

Holden N, Martin A, Owende P, Ward S. 2001. A Method For Relating GPS Performance To Forest Canopy. Int. J. For. Eng. 12:51–56.

Holopainen M, Vastaranta M, Hyyppä J. 2014. Outlook for the Next Generation's Precision Forestry in Finland. Forests 5:1682–1694.

Kaartinen H, Hyyppä J, Vastaranta M, Kukko A, Jaakkola A, Yu X, Pyörälä J, Liang X, Liu J, Wang Y, et al. 2015. Accuracy of Kinematic Positioning Using Global Satellite Navigation Systems under Forest Canopies. Forests 6:3218–3236.

Lewis JP. 1995. Fast Normalized Cross-Correlation. Vis. interface 10:120–123.

Lindroos O, Ringdahl O, Hera P La, Hohnloser P, Hellström T. 2011. Estimating the Position of the Harvester Head – a Key Step towards the Precision Forestry of the Future ? Croat. J. For. Eng. 36:147–164.

Marinello F, Pezzuolo A, Gasparini F, Arvidsson J, Sartori L. 2015. Application of the Kinect sensor for dynamic soil surface characterization. Precis. Agric. 16:601–612.

Matlab. 2017. pcregrid - ICP algorithm [Internet]. [accessed 2017 Apr 6]. https://se.mathworks.com/help/vision/ref/pcregrigid.html

Microsoft. 2017. Kinect for Windows - Kinect hardware [Internet]. [accessed 2017 Mar 2]. https://developer.microsoft.com/en-us/windows/kinect/hardware

Oliviera A, Visser R, Acuna M, Morgenroth J. 2016. Automatic GNSS-enabled harvester data collection as a tool to evaluate factors affecting harvester productivity in a Eucalyptus spp. harvesting operation in Uruguay. Int. J. For. Eng. 27:15–28.

Pagliari D, Pintoa L, Reguzzoni M, Rossi L. 2016. Integration of Kinect and Low-Cost Gnss for Outdoor Navigation. SPRS-International Arch. Photogramm. Remote Sens. Spat. Inf. Sci.:565–572.

Pierzchata M, Talbot B, Astrup R. 2016. Measuring wheel ruts with close-range photogrammetry. For. 89:383–391.

Qian C, Liu H, Tang J, Chen Y, Kaartinen H, Kukko A, Zhu L, Liang X, Chen L, Hyyppä J.

2017. An Integrated GNSS / INS / LiDAR-SLAM Positioning Method for Highly Accurate Forest Stem Mapping. Remote Sens. 9:3.

Quigley M, Gerkey B, Conley K, Faust J, Foote T, Leibs J, Berger E, Wheeler R, Ng A. 2009. ROS : an open-source Robot Operating System. ICRA Work. Open Source Softw. 3:5.

Ringdahl O, Lindroos O, Hellström T, Bergström D, Athanassiadis D, Nordfjell T. 2011. Path tracking in forest terrain by an autonomous forwarder. Scand. J. For. Res. 26:350–359.

Rosell-Polo JR, Gregorio E, Gené J, Llorens J, Torrent X, Arnó J, Escola A. 2017. Kinect v2 Sensor-based Mobile Terrestrial Laser Scanner for Agricultural Outdoor Applications. IEEE/ASME Trans. Mechatronics PP:1.

SABIC Innovative P. 2017. Lexan Margard MR5E Product Datasheet [Internet]. [accessed 2017 Apr 4]. https://sfs.sabic.eu/wp-content/uploads/resource_pdf/1362129162-18362917-Lexan-Margard-MR5E-Datasheet-2012.pdf

Schmid T, Schack-Kirchner H, Hildebrand E. 2004. A Case Study of Terrestrial Laser Scanning in Erosion Research: Calculation of Roughness and Volume Balance At a Logged Forest Site. In: Proceedings of the ISPRS Working Group VIII/2: Laser-Scanners for Forest and Landscape Assessment. ISPRS. p. 3–6.

Wiedemeyer T. 2015. IAI Kinect2 - Tools for using the Kinect One (Kinect v2) in ROS [Internet]. [accessed 2017 Apr 14]. https://github.com/code-iai/iai_kinect2

Yang L, Zhang L, Dong H, Alelaiwi A, Saddik A El. 2015. Evaluating and Improving the Depth Accuracy of Kinect for Windows v2. IEE Sensors J. 15:4275–4285.

Zennaro S, Munaro M, Milani S, Zanuttigh P, Bernardi A, Ghidoni S, Menegatti E. 2015. Performance Evaluation of the 1st and 2nd Generation Kinect for Multimedia Applications. In: IEEE International Conference on Multimedia and Expo (ICME). IEEE. Turin. p. 1–6.

Tables

Table 1. Distances measured with one and three measurement regions in infrared images.

Reference points (m)	Kinect measurements (m) 1 meas. regions / 3 meas. regions					
	T1 (1)	**T1 (2)**	**T2 (1)**	**T2 (2)**	**T3 (1)**	**T3 (2)**
4	3.90 / 3.75	4.03 / 3.96	3.96 / 3.92	4.01 / 3.89	4.36 / 3.65	10.50 / 4.38
8	8.06 / 7.80	8.14 / 8.00	7.79 / 7.71	7.96 / 7.82	10.91 / 7.97	19.37 / 9.13
12	12.01 / 11.67	12.41 / 12.15	12.02 / 11.84	12.11 / 11.92	17.40 / 12.06	25.27 / 12.90
16	16.08 / 15.66	16.33 / 16.02	15.99 / 15.77	16.13 / 15.87	23.97 / 16.67	31.40 / 17.34
20	20.65 / 20.10	20.39 / 20.03	20.44 / 20.06	20.36 / 20.03	32.25 / 21.27	35.85 / 20.87
RMSE	0.30 / 0.26	0.30 / 0.07	0.22 / 0.19	0.18 / 0.12	7.09 / 0.66	12.93 / 0.98

Track labeling: Test track 1, run 2 = T1(2)

Table 2. Comparison between speed measurements.

Test track (run)	Mean difference [±Standard deviation] (m/s)		
	Transmission - Kinect		Transmission - GNSS
	1 meas. region	3 meas. regions	
T1 (1)	0.003 [±0.019]	0.015 [±0.021]	0.022 [±0.069]
T1 (2)	0.001 [±0.032]	0.013 [±0.035]	0.064 [±0.200]
T2 (1)	0.014 [±0.027]	0.017 [±0.035]	0.035 [±0.079]
T2 (2)	0.013 [±0.025]	0.022 [±0.025]	0.068 [±0.155]
T3 (1)	0.004 [±0.135]	0.045 [±0.046]	0.074 [±0.090]
T3 (2)	-0.076 [±0.187]	0.052 [±0.044]	0.058 [±0.083]

Table 3. Difference between the Kinect depth measurements and the manual measurements.

Side	Mean difference [±Standard deviation] (mm)					
	T1 (1)	**T1 (2)**	**T2 (1)**	**T2 (2)**	**T3 (1)**	**T3 (2)**
Left	35 [±36]	38 [±27]	53 [±42]	55 [±41]	-4 [±56]	-3 [±56]
Right	29 [±25]	30 [±23]	72 [±73]	73 [±45]	19 [±67]	-45 [±55]
RMSE	44	42	86	77	62	62

Track labeling: Test track 1, run 2 = T1(2)

Figures

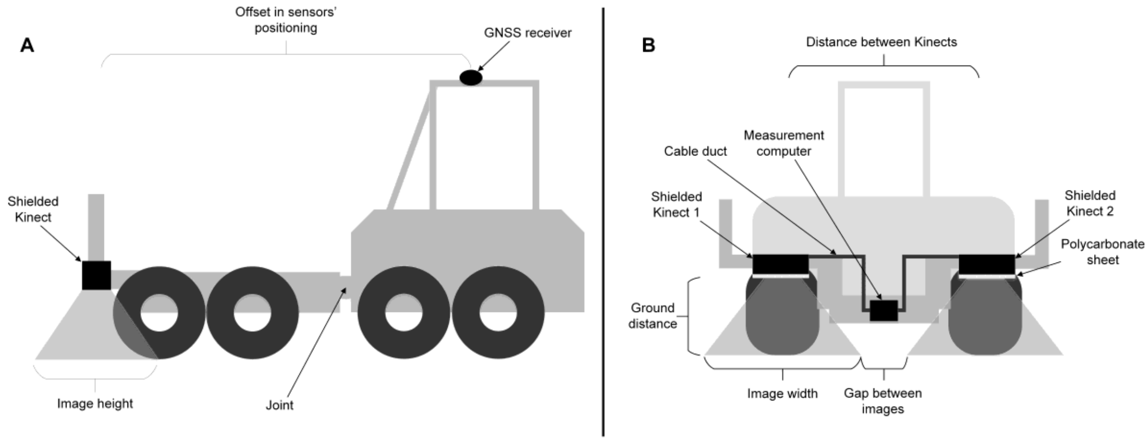

Figure 1. Kinect measurement system in the forwarder.

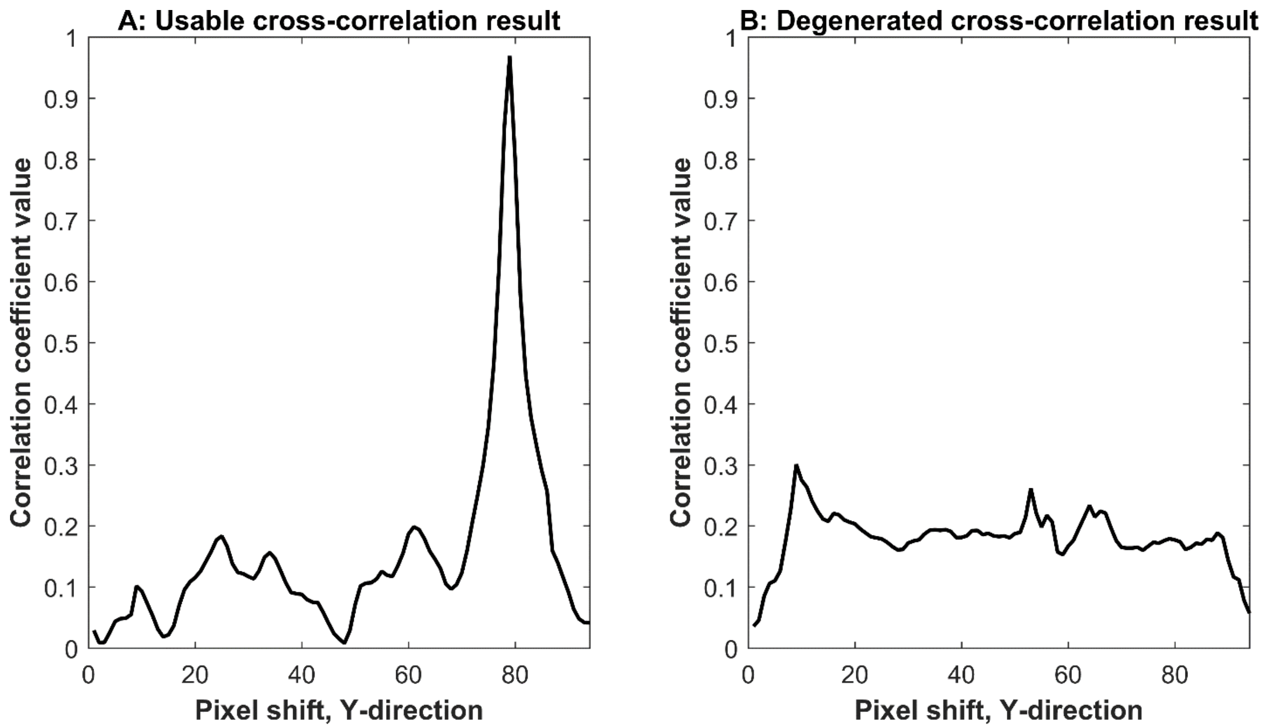

Figure 2. Examples of the normalized cross-correlation results between two consecutive infrared images in Y-direction: (a) typical result and (b) degenerated result.

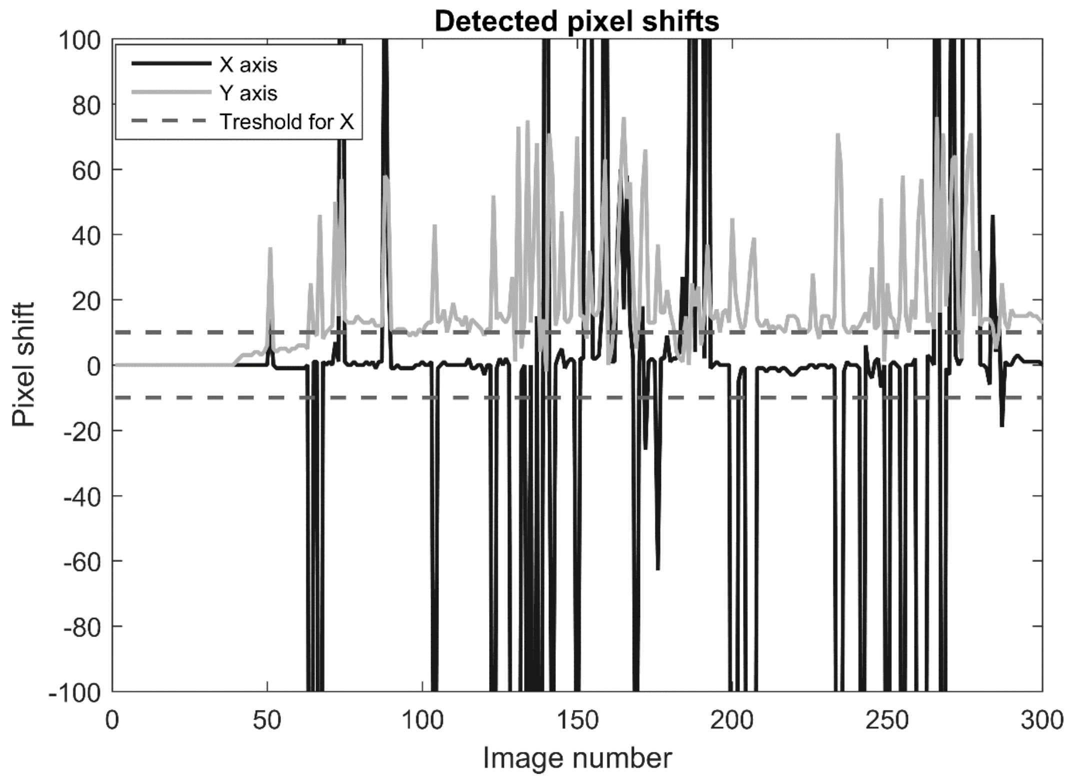

Figure 3. Detected offsets between the consecutive images in the third-track test data.

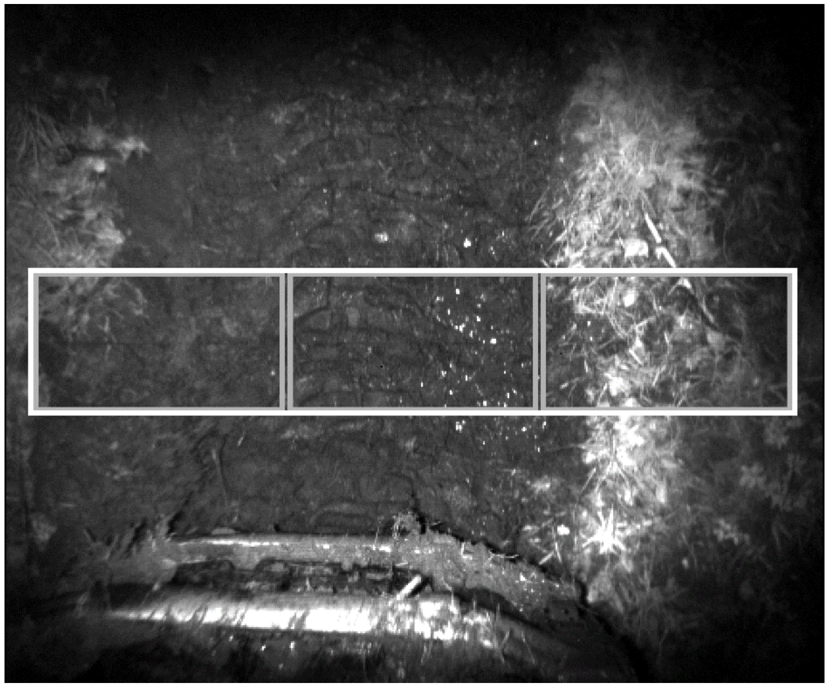

Figure 4. Measurement regions for computing the cross-correlation.

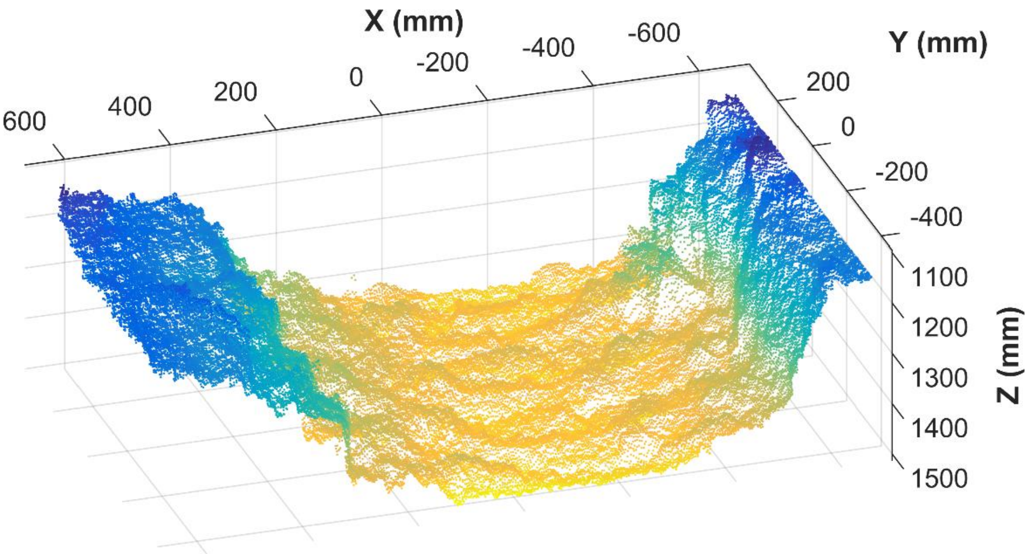

Figure 5. Soil surface profile as a 3D point cloud. The high-noise edge areas, and area with forwarder wheel have been removed.

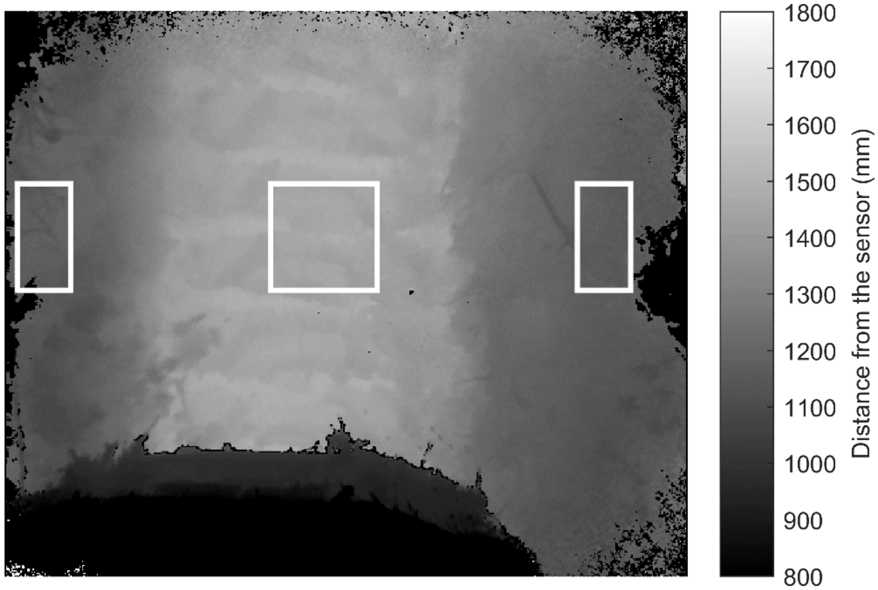

Figure 6. Depth image sections for the surface base level and rut depth measurements.

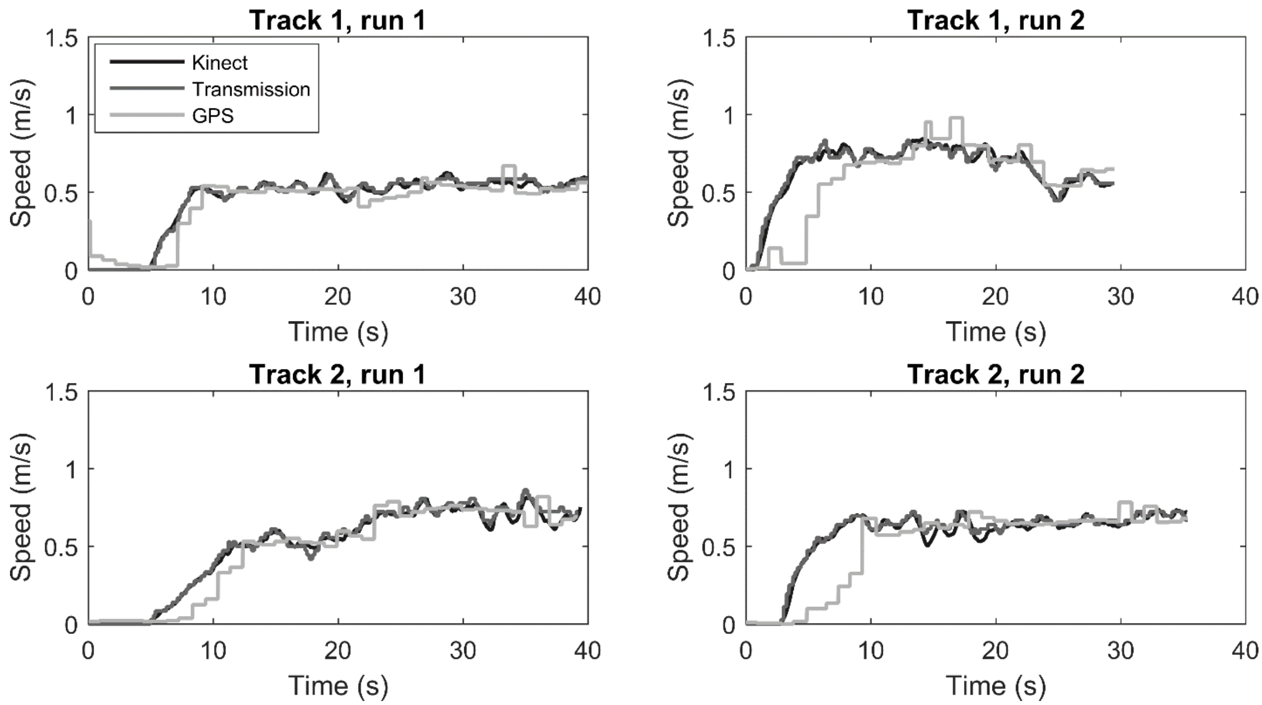

Figure 7. Measured speeds on test tracks one and two.

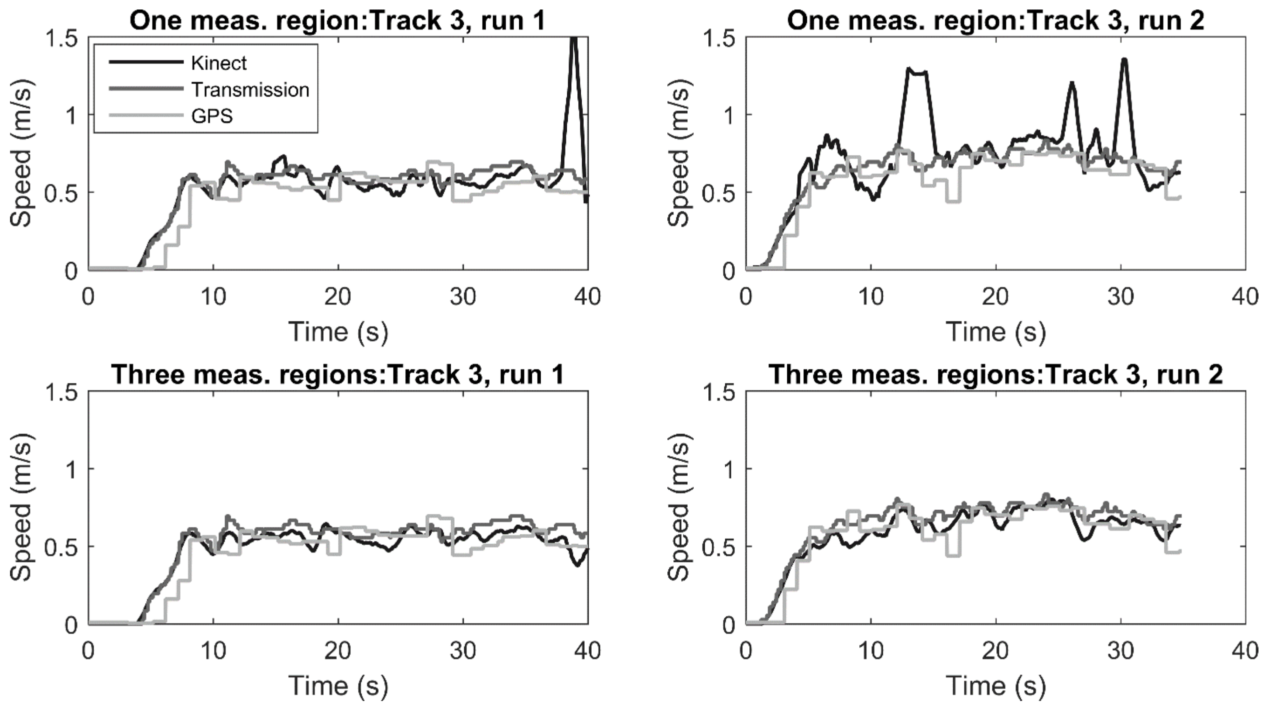

Figure 8. Measured speeds on test track three, using one and three measurement regions for the Kinect images.

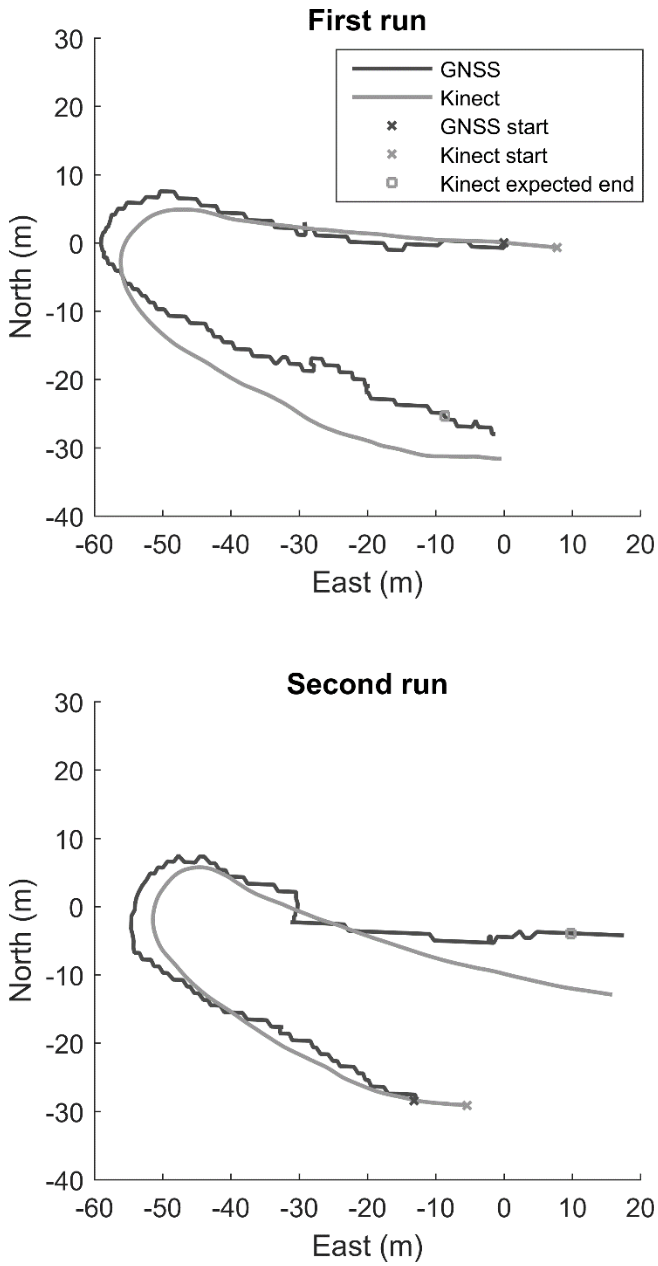

Figure 9. Forwarder position estimates using GNSS and Kinect measurements.

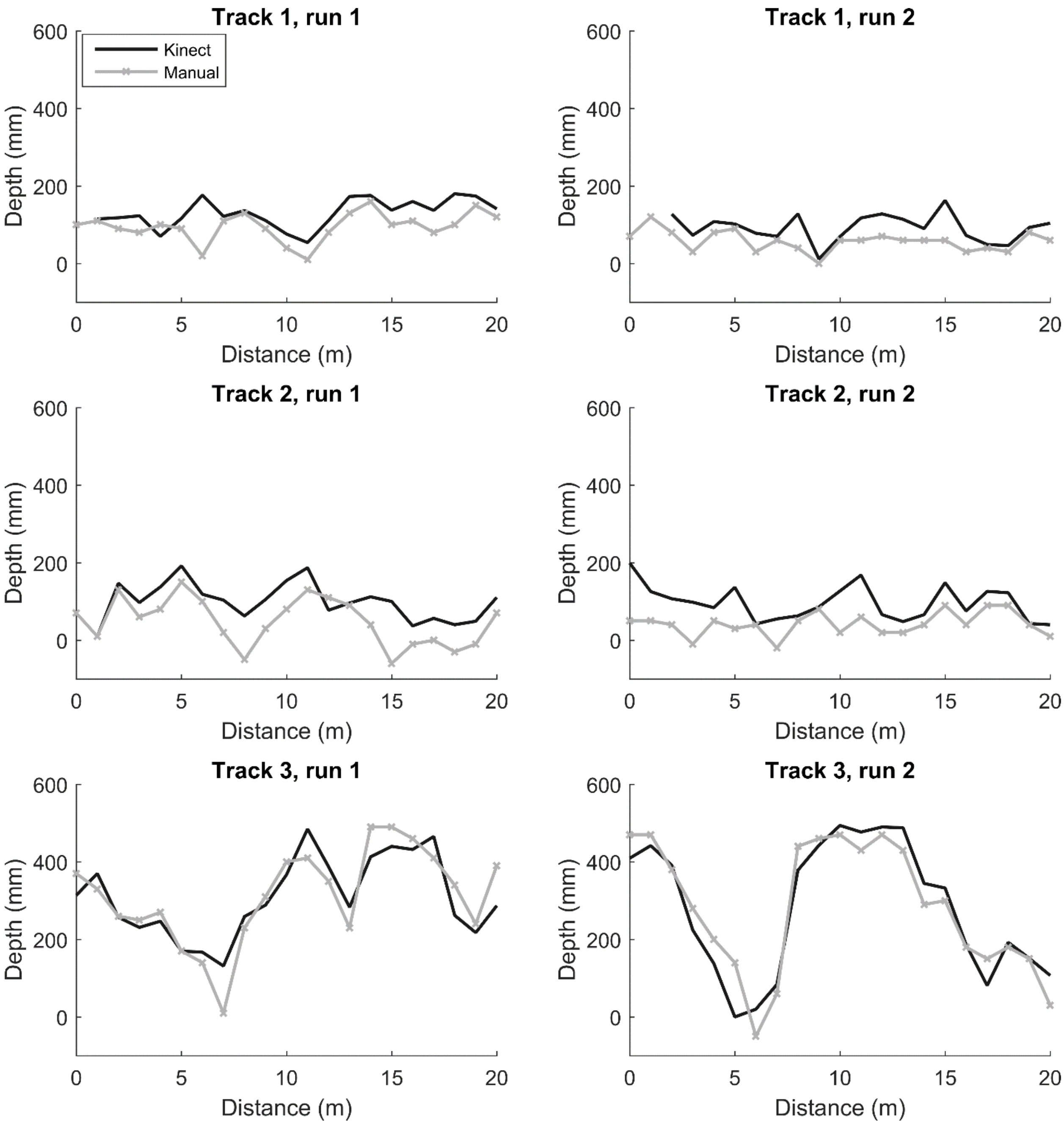

Figure 10. Measured wheel rut depths for the left side of the test tracks.